GEOLOGICA CARPATHICA, 49, 2, BRATISLAVA, APRIL 1998
85–98

DYNAMICS AND KINEMATICS OF THE CIROCHA, TRANGOŠKA AND ZÁZRIVÁ STRIKE-SLIP FAULTS, WESTERN CARPATHIANS

MICHAL NEMČOK and JÁN NEMČOK†

Slovak Geological Survey, Mlynská dolina 1, 817 04 Bratislava, Slovak Republic

(Manuscript received January 9, 1997; accepted in revised form December 11, 1997)

Abstract: The Cirocha, Trangoška and Zázrivá fault zones have dominant structures developed during the transtensional strike-slip stage of their movement histories. It is indicated by the negative flower structure on the cross-cutting reflection seismic profile and the calculated paleostress pattern from one of the three stress patterns in the case of the Zázrivá fault zone. Rotated paleocurrent sets in undefined blocks indicate the existence of flats somewhere in depht accommodating the separate block movements in the dextral strike-slip system. The most prominent structures of the Trangoška fault zone, large shear planes with striation having a significant divergent dip-slip component, were also developed during the transtensional strike-slip reactivation. It is indicated by the slickenside lineations. This sinistral reactivation did not develope shallow flats, as shown by the lack of rotations. The Cirocha fault zone acted as a dextral transtensional strike-slip during its activity. This is indicated by the calculated paleostress pattern which did not undergo significant changes. Presence of the flat at about 2.5–3 km depth is constrained by the reconstruction of the 3 km wide and 10 km long Veľká Poľana flake. This flake dextrally rotated about 90°, as indicated by the rotation of Cretaceous, Eocene and Oligocene paleocurrent patterns and paleostress patterns. This rotation was not accommodated by the formation of new faults inside the flake. These observations are compared with the shear stress/reactivation modelling. The presence of the very low friction flake boundaries would explain the fact that no new faults were formed until the flake rotated about 90°. The flat underneath the flake was developed along the flat of the pre-existing thrust fault.

Key words: Western Carpathians, strike-slip faults, fault dynamics.

Introduction

Three-dimensional strain compatibility in upper crustal levels requires steep strike-slip faults to be associated with shallow-dipping faults (Fig. 1), allowing various levels in the system to move separately (Dewey 1982; Woodcock & Fischer 1986). Such "flats", together with various steeply dipping faults in a strike-slip zone, can create fault-bounded blocks, which, under certain circumstances, could undergo uplift, subsidence and rotation. Such uplift, subsidence and rotation have been demonstrated by high resolution seismic data (Ben Avraham et al. 1979; Ben Avraham 1985), sedimentological data (Segall & Pollard 1980; Ballance & Reading 1980; Biddle & Christie-Blick 1985), earthquake data (Nabelek et al. 1987), analogue material modelling (Emmons 1969; Bartlett et al. 1981; Naylor et al. 1986), paleomagnetic studies (e.g. Luyendyk et al. 1980, 1985; Bogen & Seeber 1986; Kamerling & Luyendyk 1979, 1985; Terres & Luyendyk 1985; Hornafius et al. 1986) and described by various models (e.g. Freund 1971, 1974; Garfunkel 1974; Greenhause & Cox 1979; Lamb 1987, 1988).

Our paper aims to study the 3D strain compatibility manifestation along the strike-slip fault zones, related vertical movements and rotation, the internal deformation of rotated blocks, the origin of flats and controlling stress pattern.

We evaluate the Cirocha strike-slip fault zone involving block rotation, localized in the Flysch Belt of the eastern part of the Western Carpathians. The two other strike-slip fault zones, the Zázrivá and Trangoška zone, are evaluated for comparison.

Methods

All chosen parts of the strike-slip fault zones described below (Fig. 2), except the area in Fig. 2c, have been mapped in detail. Cave systems formed along various shear planes of the Trangoška fault zone and a strike-parallel reflection seismic profile (Kadlečík et al. 1988) through the Zázrivá fault zone allowed direct 3D study. The 3rd dimension in the Cirocha fault zone study is constructed from surface data. All available features including folds, faults, extensional veins,

Fig. 1. Dextral strike-slip fault with a flat fault accommodating its 3D deformation at Trwyn-y-Witch in the Bristol Channel region, UK. The "flat" is contoured in white, with reverse fault movement, dextral strike-slip is contoured in black.

bedding planes and sediment paleotransport vectors have been measured where possible.

Folds and extensional veins provided a rough estimate of the stress configuration which caused their origin. Fault populations outside and inside strike-slip zones have been used as input for the inversion stress routines. The methods used include the Carey & Brunier (1974) routine, Reches (1987) based method of Hardcastle (1989) and BRUTE3 software of Hardcastle & Hills (1991), providing the orientations of all three principal stresses and their ratio defined in related papers. Readers interested in details of these inversion methods are referred to Carey & Brunier (1974), Hardcastle (1989) and Hardcastle & Hills (1991).

In order to understand what happened inside the rotated block in the strike-slip zone, a field analysis was combined with fault reactivation calculations. Reactivation under applied stress configuration was simulated, in order to test what amount of rotation of the fault pattern inside the rotating block would result in new slip vectors the overprinting original ones. A set of faults measured along part of the Cirocha strike-slip fault zone was chosen arbitrarily as the test00 file. The stress configuration which controlled their displacement was computed by BRUTE3 (Hardcastle & Hills 1991). Then the same fault population was rotated about a vertical axis in 30^{o} increments. The same stress configuration was applied to these artificially made fault populations (test30, test60, test90) to calculate related shear stress vectors and compare them with measured ones using available approaches (e.g. Guiraud et al. 1989; Hardcastle & Hills 1991; Simon-Gomez 1986).

This procedure resulted in a set of slip vectors calculated for each of the three artificial populations formed by rotation of the original ones. All three new sets of slip vectors were matched against rotated original ones. Tests were done to find out, whether such a rotation of the original faults and their subsequent reactivation by the same regional stress field would be identifiable either in the field or by paleostress inversion for polyphase fault/striae data sets.

Data

The Cirocha strike-slip fault zone

The sediments affected by the Cirocha strike-slip fault zone, studied in detail, belong to the Dukla Unit (Korába & Ďurkovič 1978) of the Flysch Belt (Fig. 2a,d, 3). The Dukla Unit in the surroundings of the Veľká Poľana flake (Fig. 3), consists of a turbiditic sequence of sandstone and clay shale of Cretaceous to Early Oligocene age (Nemčok 1970, 1978; Fig. 2). This sequence, being part of the Outer Carpathian accretionary wedge, was deformed by folding and thrusting (Fig. 4a–d) with no evidence for ductile deformation in the outcrops. The strike-slip faulting, contemporaneous with, and post-dating the thrust shortening, also has a brittle character at outcrops. The Paleogene-Sarmatian age of faulting (Nemčok 1993), our estimates of the amount of shortening and far-field evaluations of erosion (Franců & Müller 1983) suggest that the mapped faults formed at depths of 2–5 km and host rock temperatures of 60–150 ^{o}C.

The Veľká Poľana flake is 3 km wide and 10 km long. It has been mapped in detail by Nemčok (1970; Fig. 3). The Cirocha strike-slip fault zone extends at least 25 km to the NE (Maheľ et al. 1973) and 45 km to the SW (Maheľ et al. 1984) of the flake. The fault zone contains Y shears trending 044–048^{o} in the Veľká Poľana area. The dextral displacement of about 5–6 km has been described by Nemčok (1970) and Korába (1983). The strike-slip fault cuts through the thrust and fold structures in a direction roughly perpendicular to the fold axes and thrust fault strikes. Adjacent blocks show slightly different structures. The western block has fold axial surfaces and thrusts dipping SW to vertical, while the eastern block has NE dipping axial surfaces and thrust planes (Fig. 5). Based on the slickensides formed on the bedding planes, both sets of folds are formed by bending with flexural slip. The flake itself has an irregular shape and no distinct offsets made by internal cross faults have been observed. Uniform paleocurrent patterns measured in three various formations inside the flake also rule out internal cross faults. A cross section through the north-eastern half of the Veľká Poľana flake gives a roughly estimated thickness for the rotated flake of about 2.5–3 km.

Collected mesoscale shear plane populations from several dozen localities can be divided into two sets. One set is related to the thrust plane pattern, which formed prior to, and contemporaneously with the strike-slip faulting along the Cirocha strike-slip fault zone. On the basis of the inversion stress computations from the thrust plane pattern made by methods of Carey & Brunier (1974), Hardcastle (1989) and Hardcastle & Hills (1991), the shortening had a NE–SW direction during the Paleogene to Sarmatian (Nemčok 1993). No significant stress rotations have been detected from the thrust pattern localized around the Cirocha strike-slip fault zone. The basic characteristics of the thrust plane pattern from the Veľká Poľana area are shown on Figs. 4a–d.

The basic characteristics of the strike-slip plane pattern along the Slovak part of the Cirocha strike-slip fault zone (Fig. 2d) are shown on Fig. 6b–e. The stress tensors computed from the rocks of various ages deformed by the Cirocha strike-slip fault zone are shown in Table 1. In addition to the shear plane populations connected with strike-slip faulting, measurements of the calcite tension veins have been collected (Fig. 7).

A more complicated situation was observed in the rotated Veľká Poľana flake. The stress tensors computed from the shear planes present at locations 2 and 5 comprise two generations. An earlier σ_1, oriented NW–SE, is perpendicular to the regional NE–SW oriented σ_1. The NE–SW oriented σ_1

Fig. 2. a — Major regional geological elements of the Western Carpathians. White — European Platform; rectangles: Zázrivá strike-slip fault zone, Trangoška strike-slip fault zone, Cirocha strike-slip fault zone. **b** — Trangoška strike-slip fault zone. **c** — Zázrivá strike-slip fault zone. **d** — Cirocha strike-slip fault zone. **e** — Zázrivá strike-slip fault zone — northern continuation.

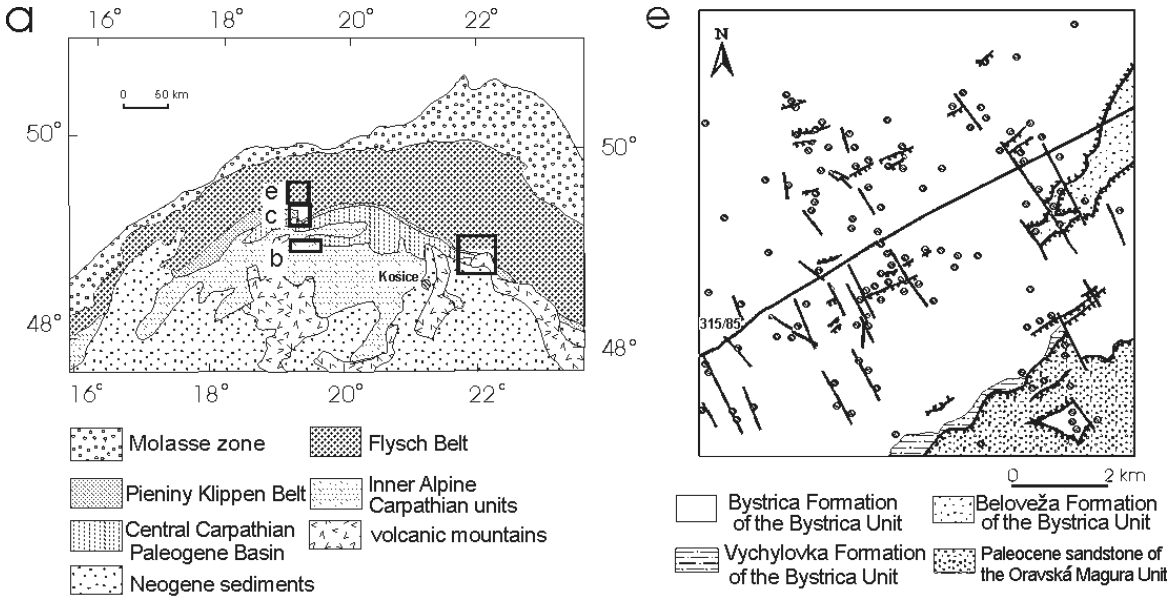
a
16°
18°
20°
22°
50°
48°
0 50 km
e
c
b
Košice
Molasse zone
Flysch Belt
Pieniny Klippen Belt
Inner Alpine Carpathian units
Central Carpathian Paleogene Basin
volcanic mountains
Neogene sediments
e
N
315/85
0 2 km
Bystrica Formation of the Bystrica Unit
Beloveža Formation of the Bystrica Unit
Vychylovka Formation of the Bystrica Unit
Paleocene sandstone of the Oravská Magura Unit

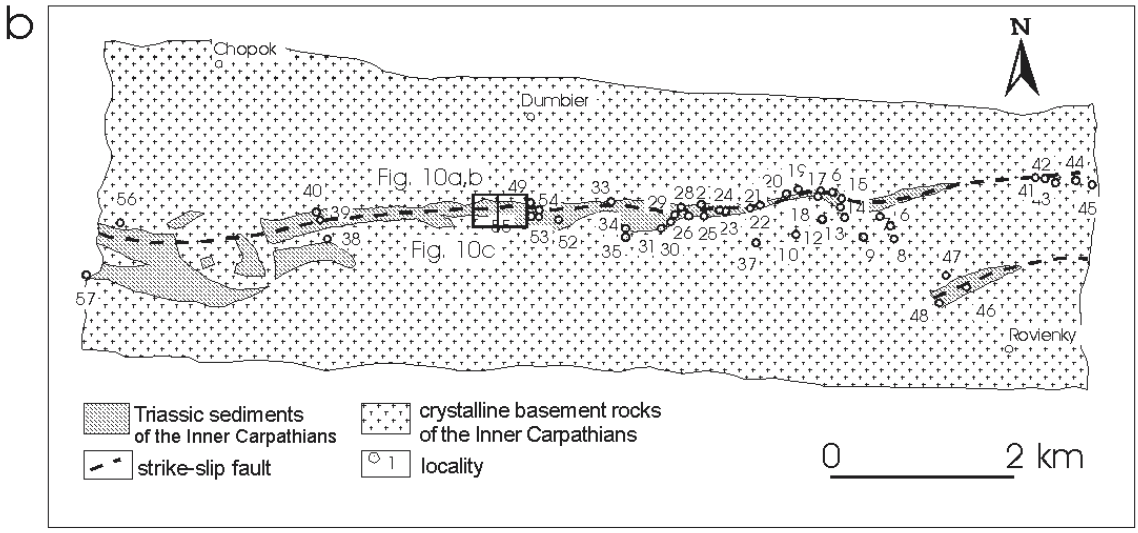
b
N
Chopok
Dumbier
Fig. 10a,b
Fig. 10c
Rovienky
Triassic sediments of the Inner Carpathians
crystalline basement rocks of the Inner Carpathians
strike-slip fault
locality
0 2 km

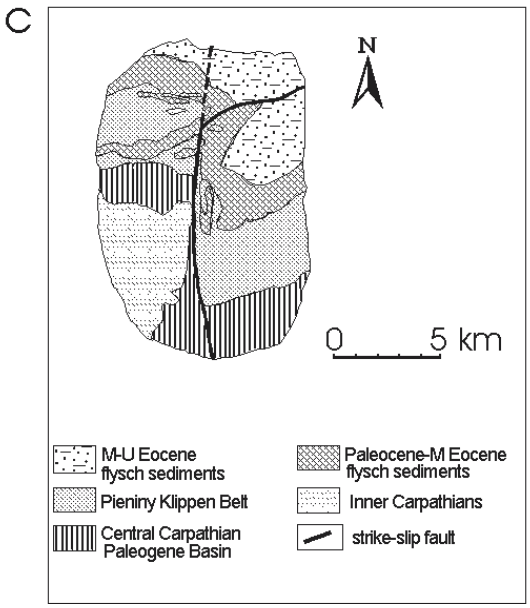
c
N
0 5 km
M-U Eocene flysch sediments
Paleocene-M Eocene flysch sediments
Pieniny Klippen Belt
Inner Carpathians
Central Carpathian Paleogene Basin
strike-slip fault

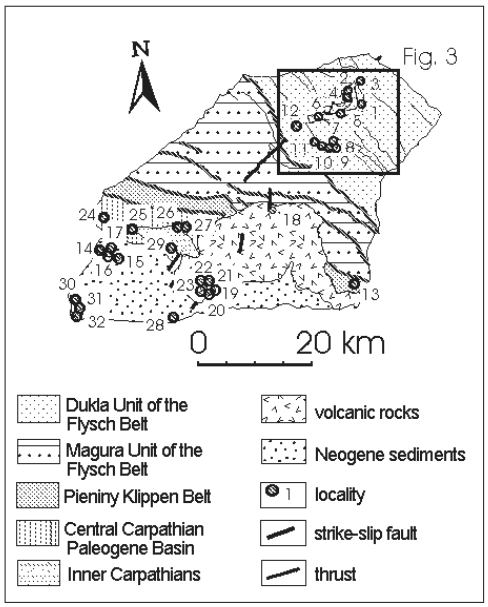
d
N
Fig. 3
0 20 km
Dukla Unit of the Flysch Belt
Magura Unit of the Flysch Belt
Pieniny Klippen Belt
Central Carpathian Paleogene Basin
Inner Carpathians
volcanic rocks
Neogene sediments
locality
strike-slip fault
thrust

Table 1

Site	Age	Rock type	Stress sigma 1	Tensor sigma 2	sigma 3	Stress ratio	Method
CZ-02	O	fl	302/27	205/14	090/59	-0.087	C&B
CZ-05	Cr	fl	155/56	055/07	321/33	-4.478	C&B
			023/30	257/45	123/30	0.100	H&B
CZ-06	Cr	fl	237/23	061/67	328/01	-2.768	C&B
CZ-07	O	fl	196/24	295/20	060/58	-0.829	C&B
			020/10	148/74	288/12	-0.750	H&H
CZ-8	Eo	fl	060/50	240/40	330/00	0.100	H&H
			060/50	263/38	164/11	0.250	H&H
CZ-11	Ec	fl	008/73	165/15	256/06	0.147	Hard
CZ-12	Eo	fl	226/40	356/37	109/28	-3.468	C&B
			006/24	243/50	111/29	-0.733	C&B
			240/50	044/39	140/08	0.150	H&B
			247/30	100/56	347/15	0.100	H&B
			247/30	043/58	151/11	0.100	H&B
CZ-13	Ti-Ne	li	000/30	096/10	202/58	0.100	H&H
CZ-15	LBa	tu	023/30	203/60	113/00	0.700	H&H
			020/10	200/80	110/00	0.700	H&H
CZ-16	LBa	tu	094/71	284/19	193/03	0.103	Hard
CZ-17	LBa	tu	002/03	270/33	096/56	0.138	Hard
CZ-18	USa	an	010/25	130/47	263/33	0.621	Hard
CZ-22	MSa	an	080/10	322/70	173/17	0.250	H&H
CZ-24	M-UTr	do	203/30	055/56	302/15	0.850	H&H
			220/10	116/53	317/35	0.700	H&H
CZ-25	Ne-AL	li	004/17	102/23	241/61	0.193	Hard
CZ-26	UTr	do	023/30	235/56	122/15	0.200	H&H
			225/30	355/48	199/26	0.150	H&H
			220/10	348/74	128/12	0.250	H&H
CZ-27	M-UEo	con	010/67	221/20	127/11	0.223	Hard
			079/42	291/44	184/17	0.904	Hard
CZ-28	UBa	an	045/30	225/60	315/00	0.600	H&H
			060/10	188/74	328/12	0.450	H&H
			240/10	122/70	333/17	0.200	H&H
CZ-29	M-UTr	do	154/70	255/04	346/20	0.100	H&H

Table 1: List of stress tensors computed from the fault populations along the Cirocha strike-slip fault zone. M-UTr indicate Middle to Upper Triassic, UTr — Upper Triassic, Ti-Ne — Tithonian to Neocomian, Ne-Al — Neocomian to Albian, Cr — Cretaceous, Eo — Eocene, M-UEo — Middle to Upper Eocene, O — Oligocene, LBa — Lower Badenian, UBa — Upper Badenian, MSa — Middle Sarmatian, USa — Upper Sarmatian. Abreviation fl means flysch rocks, con — conglomerate, li — limestone, do — dolomite, tu — tuff and an — andesite. Hardcastle & Hills (1991) and Carey & Brunier (1974) stress inversion routines have been used. Stress axes are indicated by azimuth and dip.

is present inside the flake as the younger event, recorded by cross-cutting slickenside striations (Table 1). A similar sequence is indicated by the tension veins measured by Nemčok & Nemčok (1990).

Independent evidence for block rotation has been determined by comparing paleocurrent directions from the Cretaceous, Eocene and Oligocene turbiditic sediments within the Veľká Poľana flake with those outside (Fig. 3). Paleocurrent directions have been determined by using a variety of turbiditic sole structures. Outside the flake the results show a regionally homogeneous direction, characteristic for each of the three mapped formations. The paleocurrents of each of these formations within the rotated block are also locally homogeneous, but dextrally rotated 90° (Fig. 3).

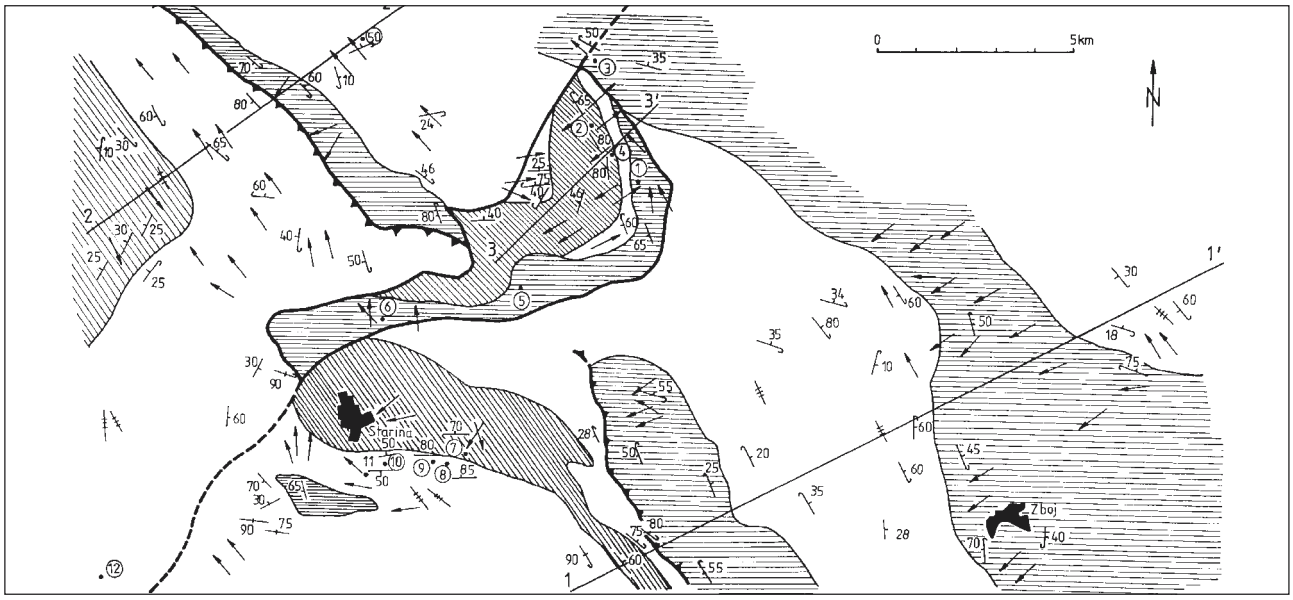

Fig. 3. Map of the Veľká Poľana surroundings, localized in Fig. 2. horizontal hachure — Cretaceous sediments; white — Eocene sediments; diagonal hachure — Oligocene sediments; straight lines — profile locations; thick lines — faults without kinematic description; thick lines with triangles — thrusts; arrows — paleocurrents; short lines crossed 3 times by shorter ones — paleocurrents without sense of transport; numbers in circles — localities; short lines with perpendicular shorter ones plus number — strike and dip of bedding planes, the normal stratigraphy of which is indicated by a little bend on the strike indicator towards the dip indicator, opposite bending indicates overturned stratigraphy.

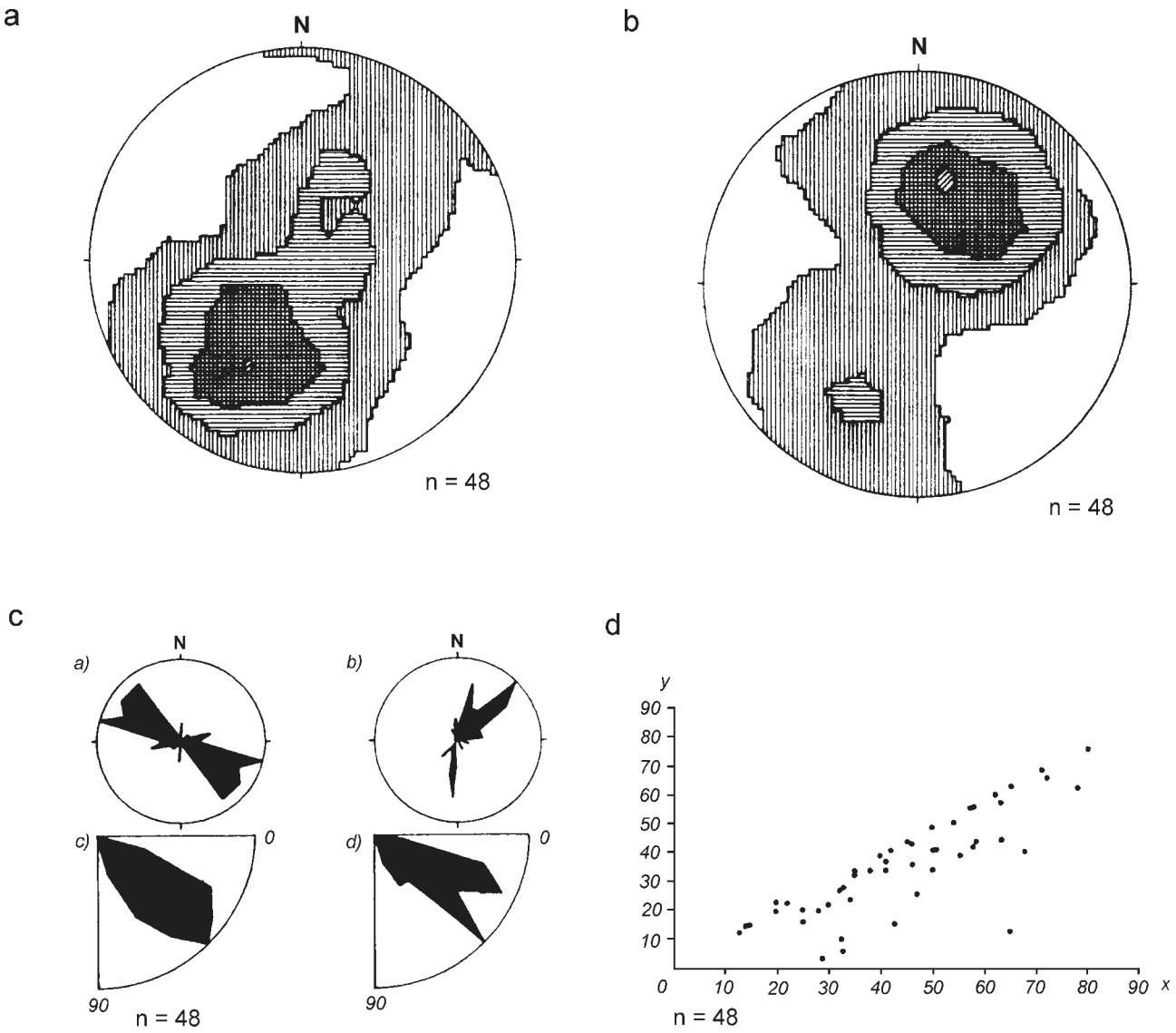

Fig. 4. Thrust planes in surrounding of the Veľká Poľana flake. **a)** Contoured diagram of the fault plane poles. Kamb contour method, counting area — 0.158, expected No. — 7.58 point per area, sigma — 2.53, contour interval — 3 sigma, vertical hachure — 1–3, horizontal hachure — 4–6, cross-cutting hachure — 7–9, thick cross-cutting hachure — 10–12, number of points — 48. **b)** Contoured diagram of the striation vectors. Kamb contour method, counting area — 0.158, expected No. — 7.58 point per area, sigma — 2.53, contour interval — 3 sigma, vertical hachure — 1–3, horizontal hachure — 4–6, cross-cutting hachure — 7–9, thick cross-cutting hachure — 10–12, number of points — 48. **c)** Rose diagrams: *a)* fault plane strikes, *b)* azimuths of striations, *c)* fault plane dips, *d)* striation plunges, number of thrusts — 48. **d)** Fault plane dip versus striation plunge diagram. Vertical axis — striation plunge, horizontal axis — fault plane dip, number of thrusts — 48.

The Zázrivá strike-slip fault zone

The Zázrivá strike-slip fault zone (Fig. 2a,c,e) was first described by Andrusov (1925), who called it the Zázrivá sigmoidal structure which he interpreted as the dextral offset of the Pieniny Klippen Belt in the northern part of the Western Carpathians (Fig. 2c). The Flysch Belt to the north of the Pieniny Klippen Belt in this area is deformed by SW-NE striking thrusts and folds. Most of the NW-SE shortening in this zone was accommodated by platform-vergent thrusting; back thrusting was only subordinate (Roth et al. 1963). The Zázrivá strike-slip fault zone was probably initiated as a lateral ramp during variable transport associated with thrusting of sediments of both the Flysch and Pieniny Klippen Belt.

The horizontal component of the displacement along the Zázrivá strike-slip fault zone is about 10 km (Haško & Potfaj 1976). The dextral displacement is indicated by the offset of the Pieniny Klippen Belt (Fig. 2c), and also by the dextral rotation of the paleocurrent system in the flysch sediments of the Flysch Belt (Haško & Potfaj 1976). The dextral displacement during the earlier stages of the activity of this fault is also indicated by structural data (e.g. Kováč & Hók 1993; Nemčok 1994). Rotations indicated by paleocurrents determined by Haško & Potfaj (1976) vary from place

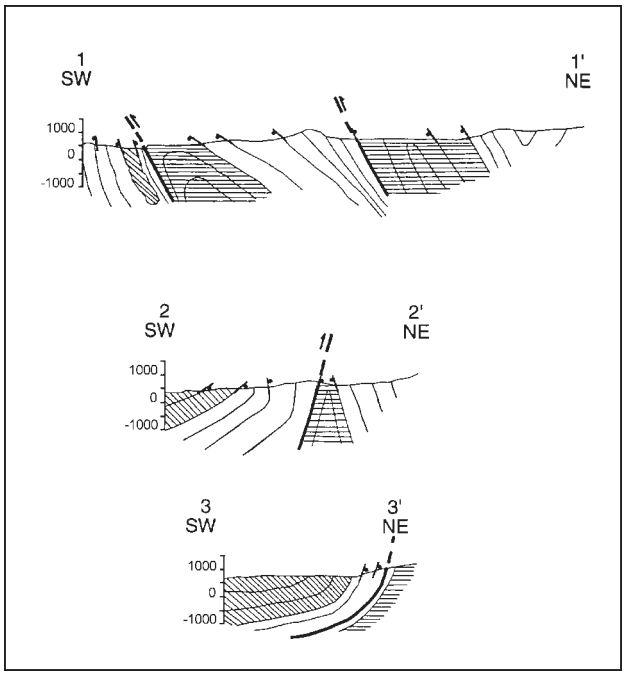

Fig. 5. Cross sections through the area of the Veľká Poľana surroundings. Horizontal hachure — Cretaceous sediments, white — Eocene sediments, diagonal hachure — Oligocene sediments, thick lines — thrusts. Localization of profiles is indicated in Fig. 3.

to place and poor outcrops do not allow the definition of the rotated blocks and their boundary faults.

The north continuation of the Zázrivá strike-slip fault zone can be studied in the reflection seismic profile 315/85 (Fig. 2e) made and interpreted by Kadlečík et al. (1988). It indicates a negative flower structure suggesting a transtensional strike-slip regime (Fig. 8). Flat lying reflectors indicate strike sections through bedding planes and thrust planes. Some of the shears forming elements of the flower structure in the profile have been studied at outcrop, where most of the related mesoscale faults indicate a strike-slip to oblique-slip movement (see Nemčok 1994). Outcrop-scale data similar to those of the Cirocha fault zone have been collected at 119 locations (Fig. 2e; Nemčok 1994) from more than 600 visited ones. Most of the fold axes are SW–NE oriented, with shallow to moderate plunge, and are related to thrusting. Smaller fold sets in the area have W-E and NW-SE striking axes. In addition, there is a significant number of vertical fold axes connected with the strike-slip faulting. Mesoscale fault populations have been used to compute stress tensors (Nemčok 1994). Extension veins have provided an additional rough check of these computations. Finally, stress trajectory maps have been constructed for the area (Figs. 9, 10; Nemčok 1994). One of maps was made assuming that the σ_1 trajectories were perpendicular to the fold axes related to the fault bend folding (Fig. 9). The other map shows the σ_1 trajectories computed from the shear plane populations. Both maps (Figs. 9, 10) demonstrate that this area was affected by three successive tectonic events. Measured paleocurrents corrected by tilt correction do not provide the regionally homogeneous pattern characteristic for certain formations. The most variable pattern is present in the Bystrica Formation of the Bystrica Unit (localized in Fig. 2e), comprising north-, northeast- and southwest-vergent paleocurrents. It indicates a rather complex fan system in time and space. A high mobility of the system is also indicated by cross-cutting relationships of flute casts on the same bedding planes, reaching a maximum difference angle of nearly 90°. This cancels the possibility of using paleocurrents as an indicator of block rotations in this area.

The Trangoška strike-slip fault zone

The Trangoška strike-slip fault zone (Kubíny 1956) strikes WSW-ENE, and deforms the Mesozoic rocks of the Central Western Carpathians in middle Slovakia (Fig. 2a,b). Our surface studies at 60 localities indicate that this fault has undergone polyphase reactivation. The last event, which caused a sinistral strike-slip displacement, created the present distinct features. It completely overprinted the previous kinematic record at some outcrops. The 3D structure of the strike-slip zone was studied thanks to 70 localities on 4 levels in the Trangoška cave system. Only 16 of them, allowed a measurement of large fault planes. Fault dip and striation plunge diagrams indicate the distinct dip-slip component of the overall movement (Fig. 11a,b), unlike the surface outcrops. The fault and bedding plane pattern in a vertical section perpendicular to the fault zone is shown in Fig. 11c and shows features similar to the flower structure of Fig. 8. A study of the fault planes utilized by the cave system shows that the majority of the faults in the deeper levels have steeper oblique-slip striations while those in the upper levels have lower angle oblique-slip or even strike-slip striations. A similar behaviour, modelled under ideal conditions, was published by Naylor et al. (1986), who have shown how the stress field controlling strike-slip faulting rotates as a function of depth (Fig. 12). This would cause a progressively more pronounced dip-slip component of the displacement on local fault planes.

Results of numerical tests

After a certain amount of rotation a fault pattern inside a rotating flake should be reactivated in order to be able to accommodate further rotation (Nur et al. 1986; Scoti et al. 1991).

In order to test this behaviour in the Cirocha fault zone case, one locality outside the fault zone cleaned from outliers was selected as a test fault population called test00. Its behaviour was investigated during simulated rotation in order to compare computed results with observations of natural faults within the rotated Veľká Poľana flake.

A stress tensor has been computed from this test00 file, having σ_1 = 195/15, σ_2 = 295/33, σ_3 = 84/53 and stress ratio $R = (\sigma_2 - \sigma_3)/(\sigma_1 - \sigma_3) = 0.1$. This stress configuration has similar parameters to other stress states computed from localities adjacent to the Cirocha strike-slip fault zone. This computed stress tensor was used to calculate a vector of maximum shear stress acting on each of the planes of our chosen

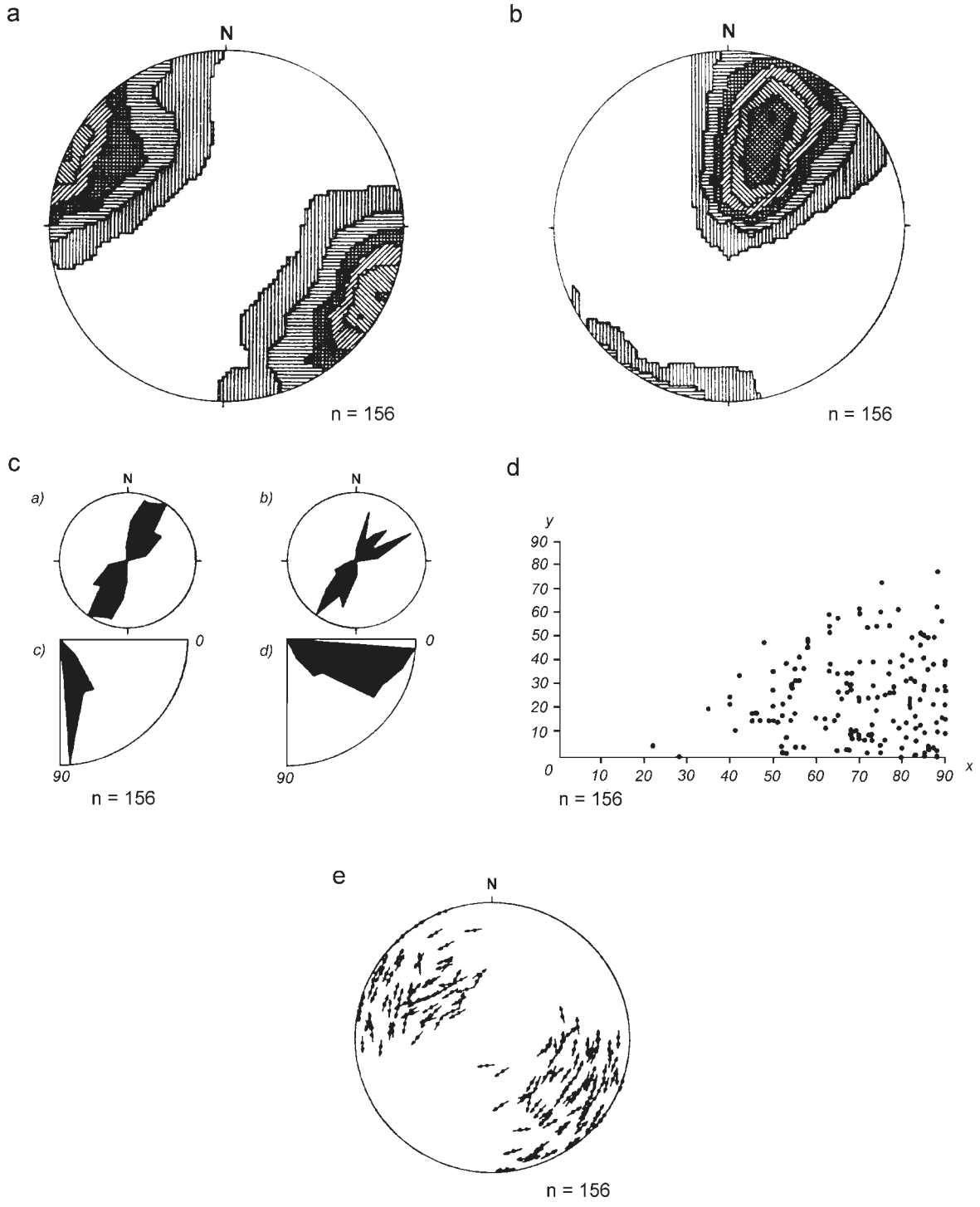

Fig. 6. Strike-slip faults of the Cirocha strike-slip fault zone. **a)** Contoured diagram of the fault plane poles. Kamb contour method, counting area — 0.055, expected No. — 8.51 point per area, sigma — 2.84, contour interval — 3 sigma, vertical hachure — 1–3, horizontal hachure — 4–6, cross-cutting hachure — 7–9, thick cross-cutting hachure — 10–12, square pattern — 13–15, right-dipping diagonal hachure — 16–18, left-dipping diagonal hachure — 19–21, number of points — 156. **b)** Contoured diagram of the striation vectors. Kamb contour method, counting area — 0.055, expected No. — 8.51 point per area, sigma — 2.84, contour interval — 3 sigma, vertical hachure — 1–3, horizontal hachure — 4–6, cross-cutting hachure — 7–9, thick cross-cutting hachure — 10–12, square pattern — 13–15, right-dipping diagonal hachure — 16–18, left-dipping diagonal hachure — 19–21, number of points — 156. **c)** Rose diagrams: *a)* fault plane strikes, *b)* azimuths of striation, *c)* fault plane dips, *d)* striation plunges, number of strike-slip faults — 156. **d)** Fault plane dip versus striation plunge diagram. Vertical axis — striation plunge, horizontal axis — fault plane dip, number of faults — 156. **e)** Hoeppner's (1955) projection of the faults. Number of faults — 156.

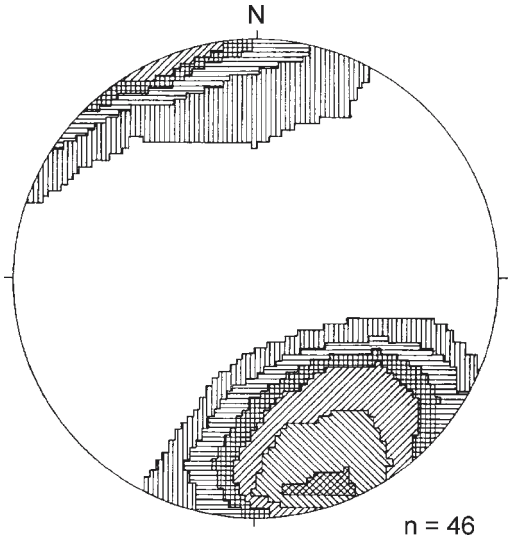

Fig. 7. Calcite tension veins in the Cirocha fault area — contoured diagram of plane poles. Kamb contour method, counting area — 0.164, expected No. — 7.53 point per area, sigma — 2.51, contour interval — 3 sigma, vertical hachure — 1–3, horizontal hachure — 4–6, cross-cutting hachure — 7–9, thick cross-cutting hachure — 10–12, square pattern — 13–15, right-dipping diagonal hachure — 16–18, number of points — 46.

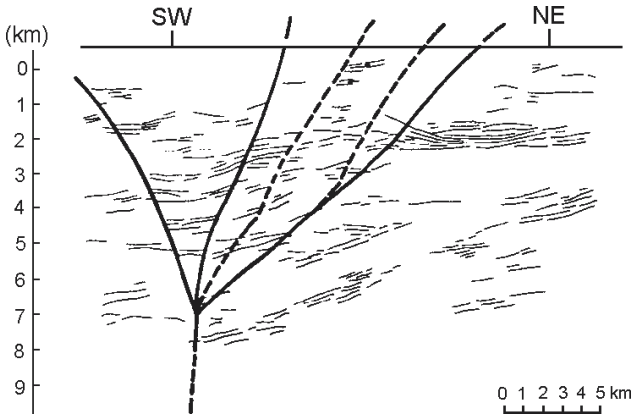

Fig. 8. Zázrivá strike-slip fault zone-flower structure in the line drawing of ENE–WSV oriented reflection seismic profile 315/85 (modified after Kadlečík et al. 1988). Thick lines — interpreted faults. SW and NE indicate related intersections of the profile with boundary of Fig. 2e. Profile is localized in Fig. 2e.

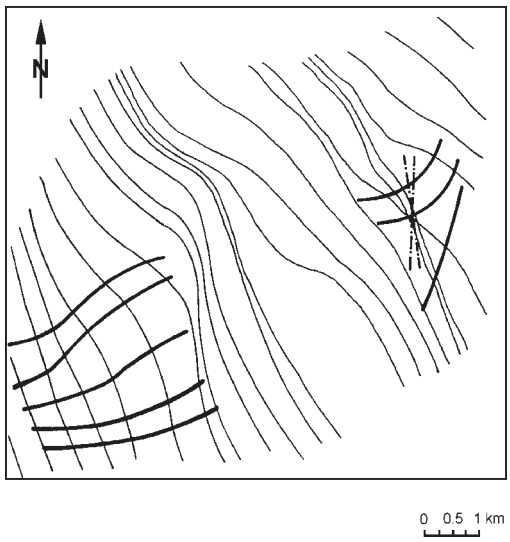

Fig. 9. σ_1 stress trajectories derived from the fold pattern along the Zázrivá strike-slip fault zone in the area of 1:25,000 map sheet M-34-87-C-d Oravská Lesná (area of the Fig. 2e). Thin lines — oldest stress field, lines with dots — younger stress field, thick lines — youngest stress field.

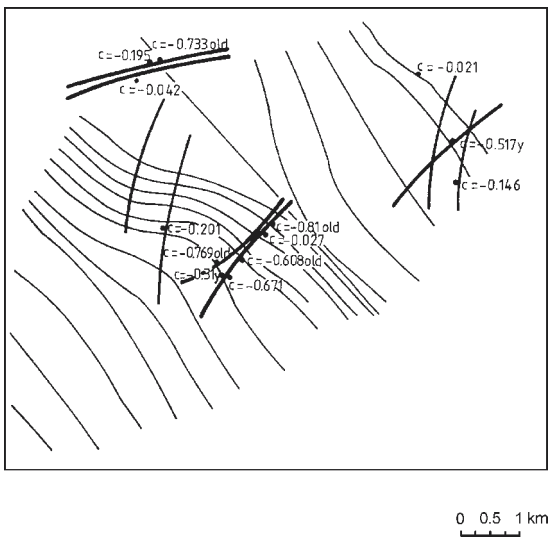

Fig. 10. σ_1 stress trajectories derived from the fault pattern along the Zázrivá strike-slip fault zone in the area of 1:25,000 map sheet M-34-87-C-d Oravská Lesná (area of the Fig. 2e). Thin lines — oldest stress field, medium thick lines — younger stress field, thick lines — youngest stress field, c — stress ratio valid for older trajectory (old) or for younger stress trajectory (y).

grid (Tables 2, 3). The vector orientation of maximum shear stress was indicated by its pitch value (Table 2) showing that the kinematics of each fault is a function of its orientation in relation to the applied stress tensor.

Then we rotated the fault planes of the test00 file clockwise in 30° increments. The fault positions in these stages were recorded as files: test30, test60 and test90.

The faults of test00 file were also tested by direct stress routine SELECT of Hardcastle & Hills (1991) to compute angular deviations of original maximum shear vectors (striations) from computed maximum shear stress vectors (Table 3). Because the measured striations were used to compute this stress tensor by an inversion technique BRUTE3 (Hardcastle & Hills 1991), the average angular deviation listed in Table 3 shows in fact the accuracy of this stress inversion.

Then we applied the same stress configuration to the fault populations: test30, test60 and test90 to see what kind of reactivation slip vector pattern is obtained in the case when

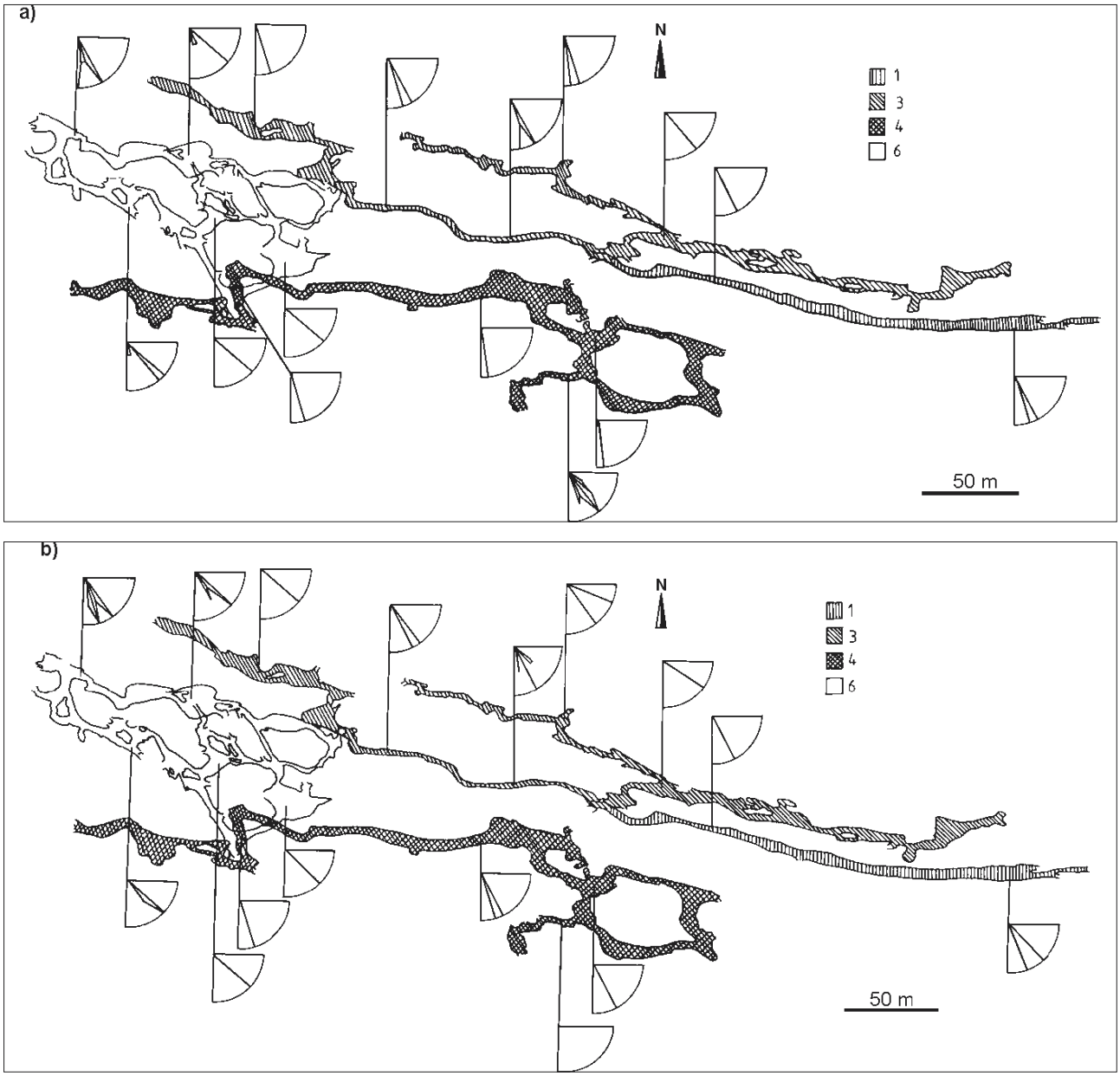

Fig. 11. Trangoška strike-slip fault zone. **a** — Map view of 4 floors of the Trangoška cave system with fault dip rose diagrams. 1 — 1st floor at 1640 m altitude, 3 — 3rd floor at 1570 m altitude, 4 — 4th floor at 1520 m altitude, 6 — 6th floor at 1420 m altitude. **b** — Map view of 4 floors of the Trangoška cave system with striation plunge rose diagrams. **c** — Flower structure interpreted from the fracture pattern in the cave system of the Trangoška strike-slip fault zone in a S-N oriented profile. Thin lines — bedding, thick lines — faults. Location of the cave is in Fig. 2b.

the stress tensor remains in the same orientation and the faults rotate. Tables 4, 5 and 6 show the angular deviations computed for the fault rotated about 30°, 60° and 90° increments. It is apparent that very large angular deviations are obtained.

Similar test with the same results was carried out using the Simon-Gomez (1986) routine, which uses an opposite approach: analysing the relation of fixed fault planes and continuously rotating stress tensor. If the regional stress configuration reactivated a rotating fault pattern inside a rotating flake it would be indicated by a new striation cross-cutting the original one on each of the faults. Thus even 30° rotation of the Veľká Poľana flake in the Cirocha fault zone should be recognized in the field by cross-cutting relationships of striae.

Table 2: Stress tensor (sigma 1 = 195/15, sigma 2 = 295/33, sigma 3 = 84/53, stress ratio (σ_1-σ_2/σ_2-σ_3) = 0.1). Pitch of maximum shear stress vector reactivated on a grid of planes. -90 indicate pure reverse faulting, 0 — pure sinistral strike-slip faulting, 90 — pure normal faulting and 180 — pure dextral strike-slip faulting.

Dip Strike	0	10	20	30	40	50	60	70	80	90
000	154	-022	-018	-012	-006	179	171	165	158	153
015	169	-009	-006	-003	178	171	162	148	122	076
030	176	177	179	-003	-018	-130	-162	-169	-173	-175
045	161	165	-001	-078	-129	-142	-150	-156	-162	-168
060	146	155	-033	-111	-124	-131	-138	-145	-153	-162
075	131	144	-068	-104	-113	-118	-123	-130	-140	-153
090	116	133	-071	-093	-098	-102	-106	-111	-118	-133
105	101	119	-061	-079	-083	-085	-086	-087	-087	-087
120	086	102	-045	-065	-069	-069	-068	-065	-059	-047
135	071	083	-019	-051	-055	-055	-053	-048	-042	-031
150	056	064	122	-035	-042	-043	-041	-038	-033	-025
165	041	045	054	172	-032	-035	-035	-032	-029	-023
180	026	028	028	026	012	-061	-042	-037	-032	-027
195	011	011	011	009	007	002	-176	-165	-145	-104
210	004	-175	-175	-176	-177	-178	-179	001	002	005
225	019	-160	-160	-162	-165	-169	-174	-180	006	012
240	034	-144	-145	-148	-152	-159	-167	-177	007	018
255	049	-128	-129	-131	-136	-144	-156	-171	010	027
270	064	-112	-112	-113	-117	-123	-135	-160	018	047
285	079	-097	-095	-094	-093	-093	-093	093	092	093
300	094	-081	-078	-074	-069	-061	-046	-016	157	133
315	109	-066	-061	-056	-048	-037	-022	-003	164	149
330	124	-051	-045	-039	-031	-021	-009	176	165	155
345	139	-036	-031	-024	-017	-008	180	171	163	157
360	154	-022	-018	-012	-006	179	171	165	158	153

Table 3

Faults are from file test00.flt

Sigma 1	Sigma 2	Sigma 3	Magnitudes			Ratio
Az /Plunge	Az /Plunge	Az /Plunge	Sigma 1	Sigma 2	Sigma 3	Sig2-Sig3 /Sig1-Sig3
195/15	295/33	084/53	5.50	1.00	0.50	0.100

Fault	data:			Comp.	values:			
Fault Str/Dip	Slicks Az/Plg	Fault class	Displ. sense	Slicks Az/Plg	Fault class	Ang. dev.	Normal stress	Shear stress
354/86	174/09	RL	1	172/22	RL	14	1.44	1.60
004/76	173/39	RLN	1	178/20	RL	19	1.19	1.09
340/82	157/24	RL	1	157/17	RL	06	2.43	2.22
168/78	177/39	RLR	1	174/28	RL	11	1.35	1.69
188/75	203/42	RLR	1	251/60	R	20	0.71	0.33
179/78	180/08	RL	1	186/31	RLR	24	0.91	1.00
180/71	187/22	RL	1	193/34	RLR	13	0.76	0.76
170/74	182/36	RLR	1	179/29	RLR	07	1.15	1.49
152/67	168/34	RLR	1	169/34	RLR	01	1.81	2.17
183/67	199/33	RLR	1	205/41	RLR	10	0.66	0.46
171/41	205/25	RLR	1	196/20	RLR	10	0.52	0.31
168/51	186/25	RLR	1	191/26	RLR	05	0.67	0.88
154/32	190/18	RLR	1	183/17	RLR	06	0.58	0.58
145/42	187/32	RLR	1	183/29	RLR	04	0.97	1.44
170/46	189/21	RL	1	195/23	RLR	06	0.57	0.57
175/77	182/29	RL	1	182/29	RLR	01	1.02	1.25
156/58	183/41	RLR	1	178/31	RLR	10	1.23	1.75
176/62	182/11	RL	1	194/30	RLR	23	0.70	0.78
166/48	185/21	RL	1	190/25	RLR	07	0.66	0.86
178/49	202/28	RLR	1	213/33	RLR	11	0.53	0.24
172/58	199/33	RLR	1	192/28	RLR	07	0.71	0.90
175/61	211/36	RLR	1	193/30	RLR	08	0.70	0.81
157/49	202/25	RLR	1	184/28	RLR	16	0.89	1.34

N = 23 Average angular deviation = 10

Prior to the block rotation induced by strike-slip faulting, a block which will be later rotated is deformed by a pattern of mesoscale faults related to the activity of the developing strike-slip fault zone. Thus, when tested by stress inversion techniques, a pattern of mesoscale faults from the rotated block provides the stress configuration synchronous with that determined from localities adjacent to the strike-slip fault zone, which did not undergo a block rotation. Such a mesoscale fault pattern rotates together with a rotated block controlled by the regional stress field, which causes the displacement along the strike-slip fault zone. Such an original mesoscale fault pattern dextrally rotated about 90° with the Veľká Poľana flake. This is the reason why the stress configuration computed from the original fault pattern indicates a stress configuration also dextrally rotated about 90° at locations 2 and 5.

When a consistent regional stress field controls the strike-slip fault zone kinematics and a randomly oriented fault plane pattern rotated inside a rotating block, each event of the internal fault reactivation should be recorded by specific cross-cutting striation on each of them. However, there is no evidence of the transmission of the stress to the rotating Veľká Poľana flake, large enough to reactivate internal faults, earlier than after 90° of dextral rotation.

Interpretation/discussion

We aim to discuss: 1) characteristic features of studied natural cases of vertical block movements and block rotation induced by strike-slip faulting, 2) the potential origin of flats underneath the rotating block, 3) internal deformation of rotated blocks, 4) when new sets of Coulomb's faults accommodating rotation have to be created and 5) what kind of stress pattern controlled the studied cases of a block rotation.

In order to discuss the first question we need to divide our studied strike-slip fault zones into distinct groups; those with and without rotated blocks.

The Trangoška strike-slip fault zone (Fig. 2b), unlike the other two zones, does not provide any evidence for block rotations. However, the Trangoška strike-slip fault zone had a lot of features similar to the other zones.

Table 3: Angular deviations of the measured and computed shear stress vectors of the file test00.flt. *Upper table* — principal stress axes positions and stress ratio of a tensor applied onto a fault pattern of test00.flt file. *Lower table* — each of the measured faults is characterized by its strike and dip of fault plane, azimuth and plunge of shear stress vector and displacement sense. RL indicates right lateral, R —reverse, RLR — right lateral with reverse component, RLN — right lateral with normal component. Each fault has indicated computed values of shear stress vector, displacement sense, acting normal and shear stress magnitudes and angle of deviation betwen measured and computed shear stress vector in the same line.

Table 4: Angular deviations of the measured and computed shear stress vectors of the file test30.flt. *Upper table* — principal stress axes positions and stress ratio of a tensor applied onto a fault pattern of test30.flt file. *Lower table* — each of the measured faults is characterized by its strike and dip of fault plane, azimuth and plunge of shear stress vector and displacement sense. RL indicates right lateral, R — reverse, RLR — right lateral with reverse component, RLN — right lateral with normal component. Each fault has indicated computed values of shear stress vector, displacement sense, acting normal and shear stress magnitudes and angle of deviation between measured and computed shear stress vector in the same line. Test30.flt file is the test00.flt file rotated about 30^0 around a vertical axis. Stress tensor is the same as in Table 5.

Faults are from test30.flt

Sigma 1	Sigma 2	Sigma 3	Magnitudes			Ratio
Az /Plunge	Az /Plunge	Az /Plunge	Sigma 1	Sigma 2	Sigma 3	Sig2-Sig3 /Sig1-Sig3
195/15	295/33	084/53	5.50	1.00	0.50	0.100

Fault data:				Comp. values:				
Fault Str/Dip	Slicks Az/Plg	Fault class	Displ. sense	Slicks Az/Plg	Fault class	Ang. dev.	Normal stress	Shear stress
024/86	204/09	RL	1	024/03	LL	168	0.97	0.64
034/76	203/39	RLN	1	210/12	LL	153	1.23	1.07
010/82	187/24	RL	1	184/34	RLN	011	0.96	0.58
198/78	207/39	RLR	1	015/12	LL	127	0.80	0.55
218/75	233/42	RLR	1	218/02	LL	139	1.64	1.86
209/78	210/08	RL	1	209/01	LL	174	1.15	1.30
210/71	217/22	RL	1	210/00	LL	158	1.20	1.47
200/74	212/36	RLR	1	018/05	LL	137	0.83	0.76
182/67	198/34	RLR	1	202/38	RLR	006	0.67	0.53
213/67	229/33	RLR	1	213/00	LL	144	1.36	1.69
201/41	235/25	RLR	1	202/01	LL	141	0.85	1.26
198/51	216/25	RLR	1	199/01	LL	151	0.75	0.99
184/32	220/18	RLR	1	200/10	LL	160	0.58	0.60
175/42	217/32	RLR	1	206/25	RLR	011	0.51	0.15
200/46	219/21	RL	1	201/01	LL	154	0.81	1.16
205/77	212/29	RL	1	024/00	LL	150	0.99	1.05
186/58	213/41	RLR	1	324/46	LLR	074	0.57	0.18
202/62	212/11	RL	1	025/00	LL	167	1.02	1.34
196/48	215/21	RL	1	198/02	LL	155	0.70	0.91
208/49	232/28	RLR	1	026/01	LL	142	1.09	1.56
202/58	229/33	RLR	1	021/00	LL	138	0.87	1.14
205/61	231/36	RLR	1	024/00	LL	136	0.98	1.29
187/49	232/25	RLR	1	005/02	LL	127	0.55	0.36

N = 23 Average angular deviation = 127

On the basis of Naylor et al.'s (1986) analogue modelling of flower structures, the one from Fig. 11c is indicative of transtension, forming just two simple branches towards the surface. This fact is also supported by the presence of a distinct amount of extensional veins and lack of the stylolites, reverse fault and fold pattern. The pure strike-slip movements combined with divergence are also indicated by a distinct dip-slip component of the displacement (Fig. 11a,b).

The Zázrivá strike-slip fault zone (Fig. 2c,e) also has also a transtensional character as supported by the negative flower structure in the reflection seismic profile (Fig. 7) and mesoscale fault data.

The situation in the Cirocha strike-slip fault zone (Fig. 2d) is rather complicated, because of mesoscale folds which are present in the rotated Veľká Poľana block, which were misinterpreted by Nemčok & Nemčok (1990) as indicative of transpression. However, this block started to rotate when NE shortening of the flysch sediments originated the Cirocha strike-slip fault zone as the tear fault, which accommodated inhomogeneous shortening and caused the dextral drag in the Veľká Poľana area. Thus the rotation happened only after a large amount of shortening. That explains the presence of folds inside the rotated Veľká Poľana block. Thus, they do not indicate the deformation of rotated block during the rotation. As a matter of fact, they underwent the same rotation as both the paleocurrent indicators and the original paleostress record. On the other hand, generations of extension veins and normal faults indicate that they formed either prior to or after the block rotation. The angle between the fault strike and σ_1 in certain cases (Table 1) also indicates transtensional dynamics of this strike-slip fault zone. However, these computations have been done most probably from various stages of the long lasting activity of the Cirocha strike-slip fault zone. That is why the local stress perturbations could change along the strike of the Cirocha strike-slip fault zone due to the local geometry changes through the time, once being transtensional, or pure strike-slip, or even transpressional, while the Cirocha strike-slip fault remained dextral from Paleogene to Sarmatian. We would not like to rule out slight changes of local dynamics along this fault zone.

The question of characteristic features is closely connected with the stress pattern controlling rotation. Knowing that the dynamics of the strike-slip fault zones was transtensional, we need to evaluate whether the stress fields controlling the displacements were regionally homogeneous. That is not the case of the Trangoška strike-slip fault zone, which was found to be reactivated by a few tectonic events. That is not the case with the Zázrivá strike-slip fault zone either inspite of the fact that this strike-slip fault zone was selected to be localized in the accretionary wedge to avoid the multiple reactivation so typical for the strike-slip faults inside orogenic belts (e.g. Christie-Blick & Biddle 1985; Gronlie & Roberts 1989), because of the following reasons. This part of the Western Carpathians was affected by changes of the stress field due to the changes in the trajectories of the orogen advance towards the European Platform (Nemčok 1993). The only strike-slip fault zone without the stress field changes is the Cirocha strike-slip fault zone. The stress controlling both the thrust shortening and the strike-slip fault zone acting as a tear fault was the same. Stress configurations computed from different stratigraphic horizons from an interval Paleogene–Sarmatian listed in Table 1 do not indicate any significant changes of orientation through time.

In order to discuss the origin of flats we will discuss a little bit more the study of the Trangoška strike-slip fault zone. There is a rough trend present, indicating the transition from the strike-slip striations to fairly steeply dipping striations as a function of depth. This situation was modelled by Naylor et al. (1986) using the sheared sand box. Authors showed a three dimensional picture of the stress field rotation which can explain the possibility of the reactivation of the pre-existing flats, increased with depth. Caused by the shear stresses ("drag") induced in the overburden by the strike-slip movement, σ_1 rotates towards being parallel with the strike of the principal displacement zone and towards the steeper

Table 5

Faults are from file test60.flt

Sigma 1	Sigma 2	Sigma 3	Magnitudes			Ratio
Az /Plunge	Az /Plunge	Az /Plunge	Sigma 1	Sigma 2	Sigma 3	Sig2-Sig3 /Sig 1-Sig3
195/15	295/33	84/53	5.50	1.00	0.50	0.100

Fault	data:			Comp.	values:			
Fault Str/Dip	Slicks Az/Plg	Fault class	Displ. sense	Slicks Az/Plg	Fault class	Ang. dev.	Normal stress	Shear stress
054/86	234/09	RL	1	232/18	LL	170	2:53	2.17
064/76	233/39	RLN	1	234/32	LLR	174	2.87	2.22
040/82	217/24	RL	1	217/14	LL	170	1.56	1.57
228/78	237/39	RLR	1	229/04	LL	145	2.32	2.21
248/75	263/42	RLR	1	248/01	LL	137	3.90	2.23
239/78	240/08	RL	1	240/05	LL	177	3:18	2.34
240/71	247/22	RL	1	059/02	LL	155	3.28	2.38
230/74	242/36	RL	1	230/01	LL	144	2:49	2.29
212/67	228/34	RLR	1	212/00	LL	143	1.30	1.64
243/67	259/33	RLR	1	060/06	LL	136	3:48	2.38
231/41	265/25	RLR	1	036/12	LL	119	2.11	2.33
228/51	246/25	RLR	1	040/09	LL	137	2.17	2.33
214/32	250/18	RLR	1	027/04	LL	133	1.25	1.78
205/42	247/32	RLR	1	024/00	LL	129	0.98	1.45
230/46	249/21	RL	1	038/11	LL	136	2.19	2.35
235/77	242/29	RL	1	235/04	LL	154	2.87	2.34
216/58	243/41	RLR	1	034/02	LL	129	1.51	1.91
236/62	242/11	RL	1	051/08	LL	158	2.89	2.43
226/48	245/21	RL	1	037/09	LL	140	2.00	2.27
238/49	262/28	RLR	1	044/15	LL	123	2.74	2.74
232/58	259/33	RLR	1	046/08	LL	128	2.54	2.40
235/61	261/36	RLR	1	050/08	LL	127	2.80	2.43
217/49	262/25	RLR	1	032/04	LL	124	1.51	1.97

N= 23 Average angular deviation =143

Table 6

Faults are from file test 90.flt

Sigma 1	Sigma 2	Sigma 3	Magnitudes			Ratio
Az /Plunge	Az /Plunge	Az /Plunge	Sigma 1	Sigma 2	Sigma 3	Sig2-Sig3 /Sig 1-Sig3
195/15	295/33	84/53	5.50	1.00	0.50	0.100

Fault	data:			Comp.	values:			
Fault Str/Dip	Slicks Az/Plg	Fault class	Displ. sense	Slicks Az/Plg	Fault class	Ang. dev.	Normal stress	Shear stress
184/86	264/09	RL	1	260/43	LLR	145	4.50	1.88
094/76	263/39	RLN	1	236/67	R	148	4.27	2.06
070/82	247/24	RL	1	244/32	LLR	171	3.51	2.24
258/78	267/39	RL	1	259/06	LL	147	4.58	1.85
278/75	293/42	RLR	1	097/01	LL	134	5.44	0.55
269/78	270/08	RL	1	271/09	LL	178	5.16	1.21
270/71	277/22	RL	1	084/15	LL	141	5.18	1.20
260/74	272/36	RLR	1	079/02	LL	140	4.71	1.76
242/67	258/34	RLR	1	059/06	LL	136	3.40	2.39
273/67	289/33	RLR	1	077/31	LLR	109	5.22	1.15
261/41	295/25	RLR	1	038/30	LLR	088	3.50	2.44
258/51	276/25	RLR	1	051/28	LLR	111	3.96	2.31
244/32	280/18	RLR	1	032/18	LLR	105	2.34	2.41
235/42	277/32	RLR	1	038/14	LL	107	2.35	2.41
260/46	279/21	RL	1	044/30	LLR	106	3.78	2.38
265/77	272/29	RL	1	266/05	LL	156	4.98	1.46
246/58	273/41	RL	1	055/16	LL	113	3.52	2.42
266/62	272/11	RL	1	068/29	LLR	133	4.81	1.72
256/48	275/21	RL	1	047/27	LLR	113	3.71	2.40
268/49	292/28	RLR	1	045/37	LLR	089	4.26	2.16
262/58	289/33	RLR	1	061/29	LLR	103	4.48	2.01
265/61	291/36	RLR	1	066/29	LLR	102	4.73	1.80
247/49	292/25	RLR	1	047/20	LL	102	3.27	2.48

N = 23 Average angular deviation =125

Table 5: Angular deviations of the measured and computed shears stress vectors of the file test60. flt. *Upper table* — principal stress axes positions and stress ratio of a tensor applied onto a fault pattern of test60.flt file. *Lower table* — each of the measured faults is characterized by its strike and dip of fault plane, azimuth and plunge of shear stress vector and displacement sense. RL indicates right lateral, R — reverse, RLR — right lateral with reverse component, RLN — right lateral with normal component. Each fault has indicated computed values of shear stress vector, displacement sense, acting normal and shear stress magnitudes and angle of deviation between measured and computed shear stress vector in the same line. File test60.flt is the test00.flt file rotated about the angle of 60^0 around a vertical axis. Stress tensor is the same as in Table 5.

dip angle in relation to the surface (Fig. 12). Thus, it can reactivate pre-existing flats, e.g. flats of the thrust planes present in the case of both the Zázrivá and Cirocha strike-slip fault zone, at a certain depth. The problem of the internal deformation of the rotated block is difficult, especially when there is no good outcrop control as occurs in the case of the Zázrivá strike-slip fault zone. The majority of studied outcrops are situated to the north of the Pieniny Klippen Belt offset, in the area without evidence of block rotations. However, this zone is not suitable for this study, because of the regional stress changes interpreted here (Figs. 9, 10). A similar outcrop situation exists in the case of the Cirocha strike-slip fault zone. There is no way to determine the exact positions of the internal faults deforming the rotated block. However, a sufficient number of outcrops provides the paleocurrent readings for three time levels: Cretaceous, Eocene and Oligocene. On the basis of the data shown in Fig. 3 and data collected by Nemčok (1970), one can see that there is a homogeneous pattern of three paleocurrent systems which excludes a possibility of more distinct deformations connected with the activity of various shears inside the rotated block. Otherwise, the internal deformation of the rotated block would be indicated by locally rotated measured paleocurrent vectors. That is why we suggest a relatively rigid block rotation here.

For the same reason we do not suggest that a new set of cross faults has to be created to accommodate rotation obeying Coulomb's law. A three dimensional block rotation model with irrotational stress directions

Table 6: Angular deviations of the measured and computed shears stress vectors of the file test90.flt. *Upper table* — principal stress axes positions and stress ratio of a tensor applied onto a fault pattern of test 90.flt file. *Lower table* — each of the measured faults is characterized by its strike and dip of fault plane, azimuth and plunge of shear stress vector and displacement sense. RL indicates right lateral, R — reverse, RLR — right lateral with reverse component, RLN — right lateral with normal component. Each fault has indicated computed values of shear stress vector, displacement sense, acting normal and shear stress magnitudes and angle of deviation between measured and computed shear stress vector in the same line. File test90.flt is the test00.flt file rotated about the angle of 90^0 around a vertical axis. Stress tensor is the same as in Table 5.

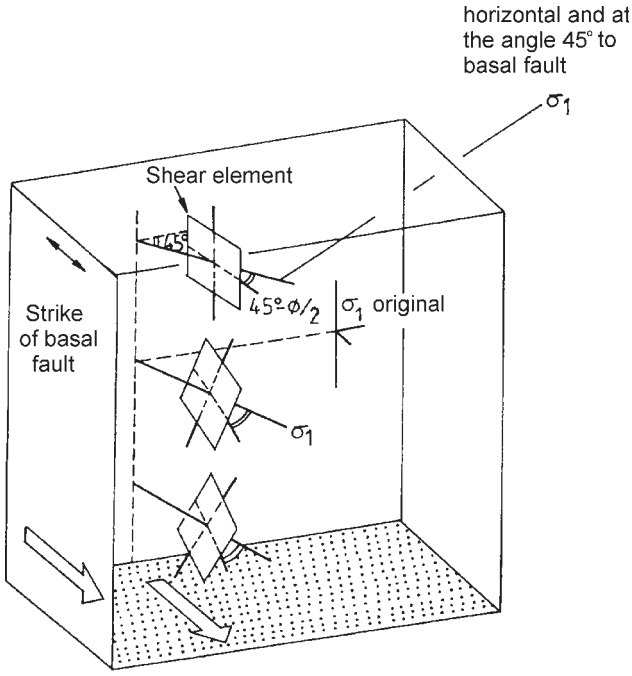

Fig. 12. 3D picture of the stress in strike-slip fault zone (Naylor et al. 1986).

through time (Scoti et al. 1991) explaining the possible rotations up to 75° can be one of the possible explanations. This requires rotation about a generally oriented rotation axis. However, this model is still unable to explain the rotations greater than 75°, which were pointed out by Mandl (1987) and indicated by our data from the Veľká Poľana flake. As noted by Mandl (1987) it seems likely in nature that, during the rotation of the first set of fractures, marginal zones of the shear band experience a reduction in shear strength — e.g. cataclasis — and, hence, will allow easier slip along the band (flake) margin. The 90° block rotation of the Veľká Poľana flake along the Cirocha strike-slip fault zone indicates a similar explanation. It could be demonstrated by the Lamb's (1987) floating block model assuming a rigid inclusion rotating in a highly viscous fluid. The case of the Veľká Poľana block rotation, in accordance with this model, is not characterized by the presence of the cross faults pinned to the strike-slip zone boundary faults. This case can be characterized rather by presence of a wider highly deformed zone bounding the rotated block which apparently allowed "unconstrained rotation" (more than the amount suggested by Nur et al. (1986) and Scoti et al. (1991)). Apart from the paleocurrent measurements, further evidence is provided by locations 2 and 5 inside the rotated block with computed initial stress configurations passively rotated roughly 90° in respect to the new stress configurations recorded as younger. This presence of new stress tensors recorded in the rotated Veľká Poľana flake implies that the friction along the boundaries of the rotated block increased up to the level which allowed the transmission of a large enough stress from the surrounding rocks to the rotating block, that is large enough to cause this calculated "new" stress tensor to be recorded. The "new" stress record has the same orientation as the regional stress in the adjacent blocks juxtaposed along the Cirocha strike-slip fault zone in various time periods. On the basis of the results of the fault reactivation modelling, each new fault motion inside the rotating Veľká Poľana flake would be recorded by newly developed cross-cutting striation of specific orientation on each of the fault planes if the large enough stress for reactivation was transmitted. The fact that such an event happened only after 90° rotation suggests that the Veľká Poľana flake rotated freely without internal faults reaching the Coulomb-Mohr conditions for reactivation. It lasted until 90° clockwise rotation, when the internal faults of the rotated block were reactivated by the regional stress controlling the overall displacement of the Cirocha strike-slip fault zone.

Summary

The transtensional character of the three cases of the strike-slip fault zones has been found during their displacement history.

Flats underneath the rotated block appear to be pre-existing anisotropies reactivated by a suitable rotated stress configuration as a function of depth.

An internal deformation of the rotated block may not occur in specific cases. Thus, a new set of cross faults needs not be created after 45° or 75° rotation to accommodate a rotation. This accommodation can be inhibited by an easier slip along the flake boundary. It can last until the boundary friction increases enough to allow a transmission of enough stress for the origin of new cross faults or reactivation of the older ones. The Veľká Poľana flake inside the Cirocha strike-slip fault zone indicates a case of a 90° rotation prior to such a reactivation.

Acknowledgements: MN wishes to thank JN who cannot see the final result, Rod Gayer whose help improved the paper considerably and Gabriela Polákova who helped with drafting. The final version of the paper was greatly improved by constructive criticism from Dušan Plašienka and a second anonymous referee.

References

Andrusov D., 1925: About sigmoidal flexion of the Klippen Belt between Orava and Kysuca. *Věstn. St. Geol. Úst.* 2, 4–6 (in Slovak).

Ballance P. F. & Reading H. G. (Ed.) 1980: Sedimentation in oblique-slip mobile zones. *Int. Ass. Sed. Spec. Pub.,* 4, 591–601.

Bartlett W. L., Friedman, M. & Logan J. M., 1981: Experimental folding and faulting of rocks under confining pressure, Part IX. Wrench faults in limestone layers. *Tectonophysics*, 79, 255–277.

Ben-Avraham Z., 1985: Structural framework of the Gulf of Elat (Aqaba), northern Red Sea. *J. Geophys. Res*., 90, 703–726.

Ben-Avraham Z., Almagor G. & Garfunkel Z., 1979: Sediments and structure of the Gulf of Elat (Aqaba) — northern Red Sea. *Sed. Geol.*, 23, 239–267.

Biddle K. T. & Christie-Blick N., 1985: Glossary-strike-slip deformation, basin formation, and sedimentation. In: Biddle K.T. & Christie-

Blick N. (Eds.): *Strike-slip deformation, basin formation, and sedimentation. Soc. Econ. Pal. Min. Spec. Publ.,* 37, 375–385.

Bogen N. L. & Seeber L., 1986: Neotectonics of rotating blocks within the San Jacinto fault zone, southern California (abs). *EOS*, 67, 1–200.

Carey E. & Brunier B., 1974: Analyse thé orique et numérique d'un mode'le mécanique élémentaire appliqué a' l'étude d'une population de failles. *C. R. Acad. Sci. Paris, sér. D*, 279, 891–894.

Christie-Blick N. & Biddle K. T., 1985: Deformation and basin formation along strike-slip faults. *The Society of Economic Paleontologists and Mineralogists Lamont-Doherty Geological Observatory Contribution No 3910.*

Dewey J. F., 1982: Plate tectonics and the evolution of the British Isles. *J. Geol. Soc. Lond.*, 139, 371–412.

Emmons R.C., 1969: Strike-slip rupture patterns in sand models. *Tectonophysics*, 7, 71–87.

Franců J. & Műller P, 1983: Organic matter maturity in Perri-Klippen Flysch of the Inner Carpathian Mts. (East Slovakia). *Geol. Carpathica*, 36, 483–494.

Freund R., 1971: The Hope fault, a strike-slip fault in New Zealand. *N. Z. Geol. Surv. Bull.*, 86, 1–49.

Freund R., 1974: Kinematics of transform and transcurrent faults. *Tectonophysics*, 21, 93–134.

Garfunkel Z., 1974: Model for the late Cenozoic history of the Mojave Desert, California and for its relation to adjacent regions. *Geol. Soc. Am. Bull.*, 85, 1 931–1 944.

Greenhause M.R. & Cox A., 1979: Paleomagnetism of Morro Rocky - Islay Hill complex as evidence for crustal block rotation in central coastal California. *J. Geophys. Res.*, 85, 2 393–2 400.

Gronlie A. & Roberts D., 1989: Resurgent strike-slip duplex development along the Hitra-Snasa and Verran faults, More-Trondelag fault zone, Central Norway. *J. Struct.Geol.*, 11, 295–305.

Guiraud M., Laborde O. & Philip H., 1989: Characterization of various types of deformation and their corresponding deviatoric stress tensors using microfault analysis. *Tectonophysics*, 170, 289–316.

Hardcastle K.C., 1989: Possible paleostress configurations derived from fault-slip data in Eastern Vermont and Western New Hampshire. *Tectonics*, 8, 265–284.

Hardcastle K.C. & Hills L.S., 1991: BRUTE3 and SELECT: Quickbasic 4 programs for determination of stress tensor configurations and separation of heterogeneous populations of fault-slip data. *Comput. Geosci.*, 17, 23–43.

Haško J. & Potfaj M., 1976: Explanations to the basic geological map of CSSR 1:25,000 M–34–99-A-b, Zázrivá. *MNS*, *GÚDŠ*, Bratislava, 1–52 (in Slovak).

Hoeppner R., 1955: Tektonik im Schiefergebirge. *Geol. Rdsch.*, 44, 26–58.

Hornafius J.S., Luyendyk B.P., Terres R.R. & Kamerling M.J., 1986: Timing and extent of Neogene tectonic rotation in the western Transverse Ranges, California. *Geol Soc. Am. Bull.*, 97, 1 476–1 487.

Kadlečík et al., 1988: Report on reflection shooting of the Flysch Belt and Inner Carpathian units 1984-88. *MNS, Geofyzika,* Brno, 1–59 (in Slovak).

Kamerling M.J. & Luyendyk B.P., 1979: Tectonic rotations of the Santa Monica Mountains region, western Transverse Ranges, California, suggested by paleomagnetic vectors. *Geol. Soc. Am. Bull.*, 90, 331–337.

Kamerling M.J. & Luyend B.P., 1985: Paleomagnetism and Neogene tectonics of the northern Channel Islands, California. *J. Geophys. Res.*, 90, 12 485–12 502.

Koráb T., 1983: Geological map of Nízke Beskydy — Východná cast 1:50,000. *GÚDŠ,* Bratislava (in Slovak).

Koráb T. & Ďurkovič T., 1978: Geology of Dukla Unit (Eastern Slovak flysch). *GÚDŠ,* Bratislava, 1–194 (in Slovak).

Kováč P. & Hók J., 1993: The Central Slovak Fault System — field evidence of a strike-slip: *Geol. Carpathica*, 44, 155–159.

Kubíny D., 1956: Report on the investigation of the central part of the Dumbier Massif. *Geol. Práce, Spr.*, 9, 110–120 (in Slovak).

Lamb S.H., 1987: A model for tectonic rotations about a vertical axis. *Earth Planet. Sci. Lett.*, 84, 75–86.

Lamb S.H., 1988: Tectonic rotations about vertical exes during the last 4 Ma in part of the New Zealand plate boundary zone. *J. Struct. Geol.*, 10, 875–893.

Luyendyk B.P., Kamerling M.J. & Terres R.R., 1980: Geometric model for Neogene crustal rotations in southern California. *Geol. Soc. Am. Bull.*, 91, 211–217.

Luyendyk B.P., Kamerling M.J., Terres R.R. & Hornafius J.S., 1985: Simple shear of southern California during Neogene time suggested by paleomagnetic declinations. *J. Geophys. Res.*, 90, 12454–12466.

Maheľ M. et al., 1973: Tectonic map of the Carpathian-Balkan mountain system and adjacent areas. Scale 1:1,000,000. *GÚDŠ*, Bratislava/UNESCO, Paris.

Maheľ M., Kodym O. & Malkovský M., 1984: Tectonic Map of Czechoslovakia. Scale 1:500,000. *GÚDŠ,* Bratislava.

Mandl G., 1987: Tectonic deformation by rotating parallel faults, the "bookshelf" mechanism. *Tectonophysics*, 141, 277–316.

Nabelek J., Chen W.P. & Ye H., 1987: The Tangshan earthquake sequence and its implications for the evolution of the North China Basin. *J. Geophys. Res.*, 92, 12 615–12 628.

Naylor M. A., Mandl G. & Sijpesteijn C.H.K., 1986: Fault geometries in basement-induced wrench faulting under different initial stress states. *J. Struct. Geol.*, 8, 737–752.

Nemčok J., 1970: Contribution to information about some tectonic alternations in East Slovakian flysh in relation to paleocurrent systems. *Geol. Práce, Spr.*, 53, 101–113.

Nemčok J., 1978: Deformations of flysch sediments as a reflection of dynamics of the basement. *Západ. Karpaty, Sér. Geol.*, 3, 35–38 (in Slovak).

Nemčok J. & Nemčok M., 1990: Significance of movement vectors in the Vihorlat-Cirocha fault system. In: Sýkora M., Jablonský J. & Samuel O. (Eds.): *Sedimentological problems of Western Carpathians.* Bratislava, 89–106 (in Slovak).

Nemčok M., 1993: Transition from convergence to escape: field evidence from the West Carpathians. *Tectonophysics*, 217, 117–142.

Nemčok M., 1994: Deformation Sequence in the Oravska Lesna Area, Flysch Belt of the Western Carpathians. *Geol. Carpathica*, 45, 185–191.

Nur A., Ron H. & Scotti O., 1986: Fault mechanics and the kinematics of block rotations. *Geology*, 14, 746–749.

Reches Z., 1987: Determination of the tectonic stress tensor from slip along faults that obey Coulomb yield condition. *Tectonics*, 6, 849–861.

Roth Z. et al., 1963: *Explanations to the well-arranged geological map 1:200,000, sheet Trstená. Geofond,* Bratislava (in Slovak).

Scoti O., Nur A. & Estevez R., 1991: Distributed deformation and block rotation in three dimensions. *J. Geophys. Res.*, 96, 12225–12243.

Segall P. & Pollard D.D., 1980: Mechanics of discontinuous faults. *J. Geophys. Res.*, 85, 4337–4350.

Simon-Gomez J.L., 1986: Analysis of a gradual change in stress regime (example from the eastern Iberian Chain). *Tectonophysics*, 124, 37–53.

Terres R.R. & Luyendyk B.P., 1985: Neogene tectonic rotation of the San Gabriel region, California, suggested by paleomagnetic vectors. *J. Geophys. Res.*, 90, 12 467–12 484.

Woodcock N.H. & Fischer M., 1986: Strike-slip duplexes. *J. Struct. Geol.*, 8, 725–735.